POLISH MARITIME RESEARCH 4 (128) 2025 Vol. 32; pp. 142-149
10.2478/pomr-2025-0057

Design and Application of Marine Robotics with a Communication Buoy

Volodymyr S. Blintsov [1]
Heorhii V. Babkin [1, *]
Dmytro V. Kostenko [1]
Volodymyr Moroz [2]
Vitalii Korobov [2]
Andrii Tarchuk [2]
[1] Admiral Makarov National University of Shipbuilding, Mykolaiv, Ukraine
[2] Institute of Hydromechanics, Kyiv, Ukraine

* Corresponding author: *gvbabkin@gmail.com (Heorhii V. Babkin)*

ABSTRACT

The basic principles of construction for a towed buoy with a arc-shaped wing are formulated and substantiated in this paper. The main characteristics of a load-bearing wing in an arched configuration are calculated, and the main dependencies and design features of the arched wing are proposed. A mathematical 3D model is built, and its hydrodynamic characteristics are mathematically modelled in the ANSYS software environment.

Experimental investigations of a half-model of an arched wing are conducted in a hydrodynamic tunnel. The model is created by 3D printing, with a Clark-Y chord profile and a tapered wingspan. The wing model is curved in an arc with a radius of 210 mm, covering a 90° sector, and is tested using a special experimental setup in a hydrodynamic tunnel in order to study the hydrodynamic characteristics of oscillating wings. This special experimental setup consists of two main blocks: a two-component strain gauge platform, and an electromechanical drive that provides the harmonic angular oscillations of the wing suspension assembly. The dependencies of the lift and drag coefficients on the angle of attack are determined experimentally. After thorough verification and calibration of the experimental setup, repeated tests are conducted on two geometrically similar wing models.

This work was conducted at the Underwater Technology Research Institute of Admiral Makarov National University of Shipbuilding and the Institute of Hydromechanics of the National Academy of Sciences of Ukraine, as part of the development of modern underwater technology prototypes. The results will be integrated into the curricula of the Admiral Makarov National Shipbuilding University.

Keywords: Wing model; Hydrodynamic characteristics; Mathematical modelling; Hydrodynamic tunnel; Experimental investigations

INTRODUCTION

Modern marine robotics tools, and particularly autonomous underwater vehicles (AUVs), are actively used for marine environment monitoring, maintenance of marine infrastructure facilities, and scientific research [1-3]. A significant proportion of these studies have been conducted in shallow coastal waters with sea depths of up to 50–100 m, where economic maritime activities are most intensive [4, 5].

One of the main considerations for an AUV operating in shallow water is the need to ensure real-time two-way video and radio communication with the shore control centre (SCC). Such communication provides the AUV with a new, beneficial feature, previously inherent only to a remotely operated vehicle (ROV), namely the "underwater presence effect" of the AUV operator. This significantly increases the productivity and quality of an underwater mission [6].

It is well known that real-time communication between an AUV and the SCC can be implemented using a system of autonomous radio buoys equipped with positioning systems and an acoustic channel for communication with the AUV [7]. One drawback of this communication method is the need to use several radio buoys, which complicates its practical operation. Moreover, the bandwidth of the acoustic communication channel between the AUV and the buoy is insufficient for the simultaneous transmission of data from the vehicle's video cameras and sonars. An alternative option for establishing communication between the AUV and the SCC is the use of acoustic modems, which convert digital data into acoustic signals that then propagate through the water [8]. However, this method has a limited scope for application to communication between an AUV and the SCC due to its high cost, and extra equipment is required when the underwater vehicle operates far from the shore.

The use of very low frequency electromagnetic signals is also promising [9]. However, suiTable equipment for their application is currently under development, and the bandwidth is expected to be low. A simpler solution may involve the use of a towed buoy (TB) as part of an autonomous vehicle, which is equipped with transceiver equipment and antennas for communication between the AUV and the SCC [10]. In this configuration, the AUV is fitted with a winch of tow cable (WCT), which allows for adjustments to the length of the deployed tow cable (TC) according to the depth of the water area and the speed of the AUV (Fig. 1).

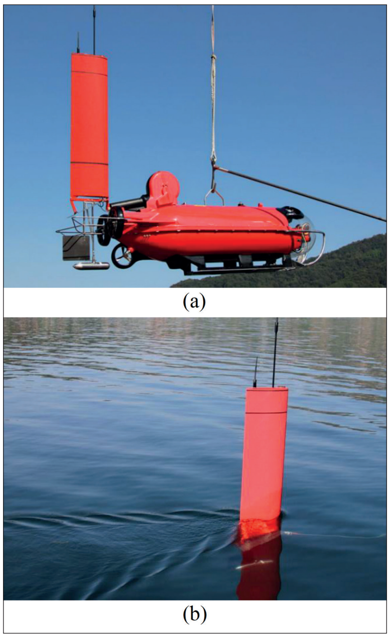

Fig. 1. Photographs of the AUV "Pluto Plus" [10]; (a) preparing for descent (b) moving with a buoy

However, the aforementioned technical solution has several drawbacks, with a noTable example being the placement of the TB outside the AUV's hull, as this complicates the operation of the AUV and increases its frontal hydrodynamic drag. The latter disadvantage results in reduced autonomy of the AUV in cases where communication with the SCC is required only periodically, while the majority of the underwater mission is conducted in autonomous mode.

This paper presents a new design for the TB in the form of a cylindrical body equipped with bearing surfaces (wings) in the shape of an arc, the radius of which is equal to the that of the AUV's outer hull (Fig. 2). A towing winch is installed on board the vehicle, which allows for adjustments to the length of the TC to ensure the optimal position of the buoy. The buoy with communication equipment is towed behind the vehicle at a given speed (Fig. 2(a)). The buoy is designed in such a way that at a given towing speed, an additional lifting force acts on it, raising it above the water surface. In the case where the use of the buoy is not necessary, the towing cable is reeled in, and the buoy is placed in the cradle on the vehicle hull, as shown in Fig. 2(b). To reduce the impact on the movement of the vehicle when the buoy is removed, its shape and outer surface mimics the surface of the hydrodynamic fairing of the vehicle itself.

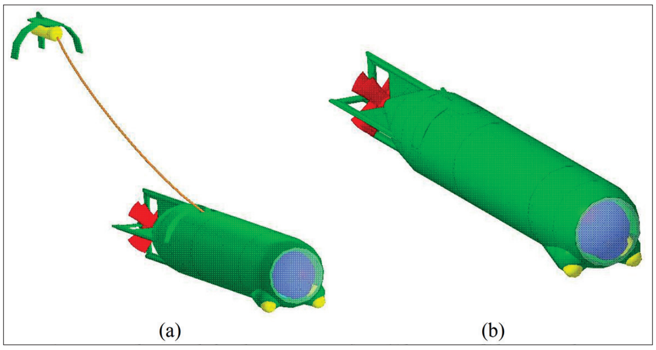

Fig. 2. Autonomous underwater vehicle with a communication buoy: (a) buoy towing, (b) buoy retracted

PREVIOUSLY UNSOLVED ASPECTS OF THE GENERAL PROBLEM

Until now, the hydrodynamics of underwater wings has been considered only in the context of the design of dynamically supported vessels, with a specific focus on hydrofoil ships. However, an arcuate wing has never been considered [4, 11]. An arched wing was considered for the first time by a engineer called Willard Ray Custer (Pennsylvania, USA) [12], who created the first model with a wing in an arched configuration and received a patent in 1926. This model confirmed Custer's assumptions, and generated substantial lift at low speeds. In theory, a fully fledged airplane of this type would be able to take off almost vertically, with a very short run-up, and all that remained was to implement the scheme in the patent [12], but in practice the patent was not implemented. Subsequently, the arched wing configuration was considered exclusively in relation to aircraft.

OBJECTIVE, METHODS, OBJECT AND SUBJECT OF RESEARCH AND PROPOSED SCHEME

The aim of this study is to formulate and substantiate the scientific principles for creating marine robotics with the use of a load-bearing wing.

The research was carried out using modern methods and processes of design and manufacture of marine robotic systems.

When moving in the water column, the main forces acting on the buoy are as follows (Fig. 3):

- G – gravitational force applied at the centre of mass of the buoy, which is directed towards the ground and does not participate in motion control;
- F_A – buoyancy force applied at the centre of mass of the buoy, which is directed upward and does not participate in motion control;
- Y – hydrodynamic lifting force;
- X – force of frontal resistance (drag force);
- P –thrust force, which is generally directed along the main structural axis of the buoy; its line of action may not pass through the centre of mass, and may be located above or below it;
- R_A – resultant hydrodynamic force, which never passes through the centre of mass.

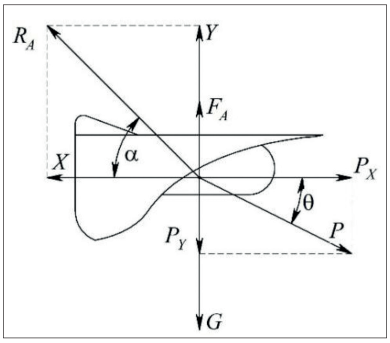

Fig. 3. Forces acting on the buoy

The transfer of the thrust force and the hydrodynamic force to the centre of mass, in accordance with the principles of mechanics, results in the appearance of a thrust moment and a hydrodynamic moment. The resultant moment of these forces, as a vector, can be projected onto the axes of the associated coordinate system (0*x*, *y*, *z*); in this coordinate system, the *x*-axis is directed along the longitudinal structural axis of the buoy, the y-axis lies in the vertical plane of symmetry of the buoy and points upward, and the *z*-axis is directed toward the right wing. The projections of the resultant moment onto the *x*, *y*, and *z* axes are referred to as the roll, sway, and pitch moments, respectively, and are denoted as M_x, M_y, and M_z. In buoy hydromechanics, the pitch moment receives the most attention, since the majority of buoy manoeuvres occur in the vertical plane, involving ascent and descent, straight-line motion, and depth adjustment.

To implement various modes of motion, complete or partial equilibrium of the external forces and moments acting on the object is required. The equilibrium conditions can be written as follows:

$$\Sigma X = 0 \quad \Sigma M_X = 0$$
$$\Sigma Y = 0 \quad \Sigma M_Y = 0$$
$$\Sigma Z = 0 \quad \Sigma M_Z = 0 \tag{1}$$

In steady horizontal motion:
- the left side of each equation will be equal to zero (i.e. the velocity is constant and does not depend on time);
- the inclination angle of the trajectory is equal to zero, and does not change (horizontal motion);
- $\cos\alpha = 1$, $\sin\alpha = 0$ (i.e. the angle of attack is small).

In other words, the following conditions are satisfied:
- the depth constancy condition $H = const$

$$Y + F_A - G - P_Y = 0 \tag{2}$$

- the constant velocity condition

$$P_X - X = 0 \tag{3}$$

The wing shape is determined by the need to minimise the hydrodynamic resistance of the AUV in the passive buoy mode. When the buoy is inactive, it occupies a position in the cutout of the AUV's hydrodynamic fairing, which allows the overall dimensions of the AUV to remain unchanged and enables it to operate at the maximum possible speed. In the case where a buoy with a conventional wing is used, its placement on board the AUV would require a dedicated hangar structure; this would increase the AUV's dimensions and alter its hydrodynamic characteristics, since, according to theory, the drag of the protruding parts includes both frictional drag and form drag, and can make up a significant proportion of the total hydrodynamic resistance (up to 30–40%) [13]. In this case, to ensure the best hydrodynamic characteristics at a low towing speed, the wing shape is chosen as trapezoidal (Fig. 4).

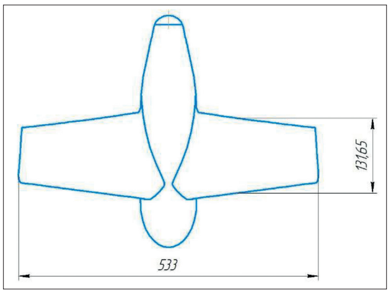

Fig. 4. Overall dimensions of the buoy wing

The wing area is calculated as follows:

$$S_{wing} = 2 \cdot \frac{b_k + b_o}{2} \cdot \frac{l}{2} = l \cdot b_{avg} =$$
$$= 0.533 \cdot 0.13165 = 0.07 \text{ m}^2. \tag{4}$$

The wing aspect ratio is then

$$\lambda = \frac{l}{b_{avg}} = \frac{533}{131.65} = 4.05\,, \tag{5}$$

and the wing taper ratio is

$$\eta = \frac{b_o}{b_k} = \frac{163.3}{100} = 1.633\,. \tag{6}$$

According to theory, the wing taper ratio for low-speed motion should not exceed three.

When analysing the lift force formation (Fig. 5), it can be observed that toward the wingtip, the direction of the lift force changes, and that it acts almost horizontally at the very tip, directed toward the body of the buoy.

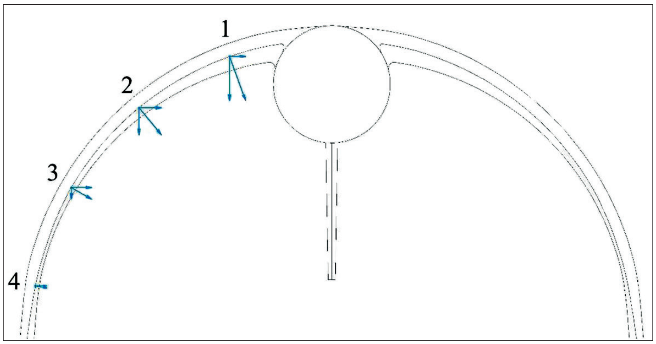

Fig. 5. Lift force formation along the wing: (1) ϕ=20°; (2) ϕ=40°; (3) ϕ=60°; (4) ϕ=80°

Hence, during towing, vortices will form at the wing tips, which will affect the course stability of the buoy. In addition, the horizontal component of the lift force at the wing tips will generate a torque that adversely affects the buoy's stability during motion.

If we assume that the angle of attack does not change, then, according to Zhukovsky's theory [11], the dimensionless lift coefficient C_y along the entire length of the wing will be constant. The lift of the wing is then determined as

$$Y = \frac{1}{2} C_y S \rho U^2 , \tag{7}$$

and will have a constant value, and the horizontal and vertical components of the lifting force will be

$$Y_x = sin\,\phi Y , \tag{8}$$

$$Y_y = cos\,\phi Y , \tag{9}$$

where ϕ is the angle of deviation of the lifting force from the vertical.

In this case, the dimensionless coefficient of the lifting force is

$$C_y = 2m(\alpha - \alpha_0) \tag{10}$$

where:

α – angle of attack;

α_0 – angle of attack at which lift is zero;

m – coefficient depending on the shape of the wing profile.

The results of the preliminary evaluation calculation are given in Table 1.

A comparison of the effective torque for a fixed angle of attack and for an angle of attack that changes along the length of the wing is given in Table 1. From this table, it is clear that the torque in the latter case is significantly reduced, whereas at a fixed angle of attack, the torque constantly increases.

To simplify the design of the buoy and to reduce its mass-dimensional characteristics, the wing is not mechanised. In addition, to reduce the influence of vortex formation on the trajectory of motion and decrease the loading on the wing tips, an aerodynamic twist was incorporated into its design: as the angle of attack changes gradually along the span of the wing, and at a deflection angle of 15° from the horizontal plane, the wing profile also changes.

The main airfoil used for the wing is based on a TsAGI R-11 profile with a relative thickness of 0.12. At the wing root, the angle of attack is α = 5°. At intervals of 15°, the angle of attack decreases by 1°, and as the angle of attack approaches zero, the wing profile becomes a SIBNIA profile with a relative profile thickness of 0.12. In this approach, the wing tips act as course stabilisers, and together with the tail stabiliser, should ensure the stabilisation of the buoy during straight-line motion. The airfoil data were obtained from [14].

MATHEMATICAL MODELING

Hydrodynamic modelling of the constructed 3D model was carried out in the ANSYS 2023 software environment [15, 16]. Fig. 6 shows the simulation results.

Two grid zones were created, in the form of tetrahedra. The first, which forms the simulation space, had a large cell size to reduce the calculation time, whereas the space nearer the model had a much smaller cell size, to increase the accuracy of the calculation. In total, 245,898 cells were created.

A standard k-epsilon turbulence model with the heat transfer parameter turned on was chosen for the simulation, with a flow velocity of 3 m/s and 5% turbulence. The simulation medium was water, and 100 iterations were used in the calculation.

Experimental studies were conducted in the small hydrodynamic tube at the Department of Hydro-bionics and Boundary Layer Control at the Institute of Hydromechanics, NAS of Ukraine [17]. This is a closed-circuit facility that was designed for the study of the hydrodynamic characteristics of bodies in a reversed flow. The flow speed could be adjusted from 0.1 to 2.5 m/s, and the working section of the tunnel was a rectangular segment with internal dimensions of 400×400×1800 mm. The bottom was made of stainless steel, while the top and side walls were made of 10 mm thick acrylic glass. To straighten the flow at the nozzle inlet, a honeycomb

Tab. 1. Preliminary estimations for the lift force components

Point	Angle ϕ, degrees	sinϕ	cosϕ	Angle α, degrees	Shoulder *h*, *m*	Components of lifting force *Y*, *N*				Torque *M*, *Nm*	
						No change α		With a change α		No change α	With a change α
						Y_x	Y_y	Y_x	Y_y		
1	20	0342	0.939	4.36	0.090	71.77	197.19	62.58	171.95	6.46	5.63
2	40	0.642	0.766	3.19	0.166	134.88	165.75	86.06	102.56	12.14	7.75
3	60	0.866	0.5	2	0.239	181.73	104.92	72.69	41.67	16.36	6.54
4	80	0.984	0.173	0.04	0.306	206.66	36.44	1.65	0.29	18.6	0.149

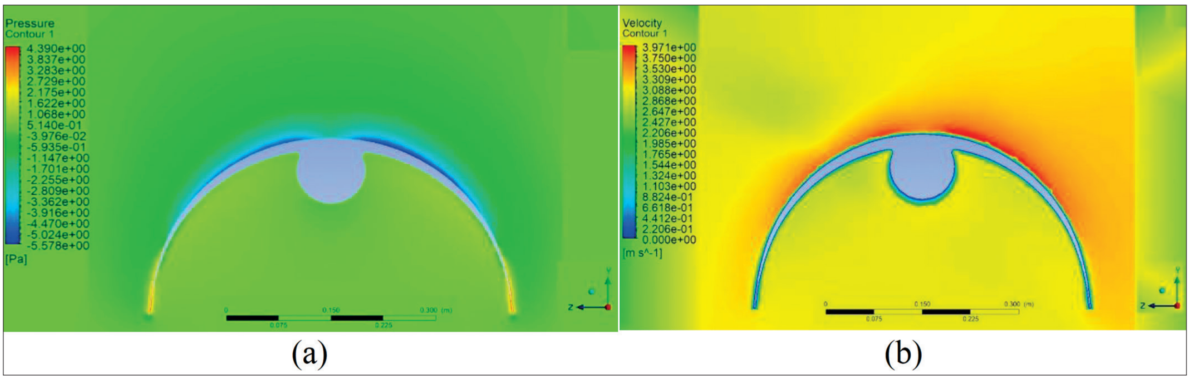

Fig. 6. (a) Pressure distribution and (b) velocity variation along the wing focus line

with cell dimensions of 25×25×60 mm was used. This nozzle provided a fivefold flow compression, and its wall profiles were designed according to Vitoshynskyi's formula [18]. On the lid of the working section of the tunnel, there was a rectangular well (250×350 mm), used for loading test models into the working area.

An external view of the hydrodynamic facility with the control system is shown in Fig. 7.

Fig. 7. External view of the hydrodynamic facility with the control system

For the experiments, a mock-up of a curved arched wing was made, a sketch of which is shown in Fig. 8(a). This wing model was produced using 3D printing, and had a Clark-Y chord airfoil profile [18]. The wing had a taper along the span, with the root chord measuring b_{root} = 153 mm and the tip chord measuring b_{tip} = 95 mm. Thus, the mean aerodynamic chord of the wing was $b_{mah} = (b_{root}+v)/2 = 0.124$ m. The mock-up was curved along an arc with a radius of 210 mm, covering a 90° sector (see Fig. 8(a)).

A rectangular thin shim measuring 55×182 mm, with rounded corners, was attached to the root chord of the wing (see Fig. 8(b)). The root chord was rotated relative to the longitudinal axis of the shim by an angle of δ_{root} = 5.2°, corresponding to the installation angle of the wing on the hull of the underwater vehicle. This shim prevented fluid from flowing between the lower and upper surfaces of the wing, which also helped in simulating the kinematic flow conditions around the wing in the presence of the hull. In addition, the presence of the shim simplified the determination of the wing's orientation in the flow (relative to the long side of the shim). An M8 threaded stud was installed at a distance of 45 mm from the wing tip, which served as a fastening element for the wing mock-up to the experimental setup and as the axis of rotation for the wing.

Tests of the wing model were conducted with a specialised experimental setup used in the hydrodynamic facility for studying the hydrodynamic characteristics of oscillating wings [19]. The setup consisted of two main components: a two-component strain gauge platform, and an electromechanical drive that provided the harmonic angular oscillations of the wing suspension unit.

A schematic diagram of the experimental setup and its arrangement within the working section of the hydrodynamic tunnel are shown in Fig. 9.

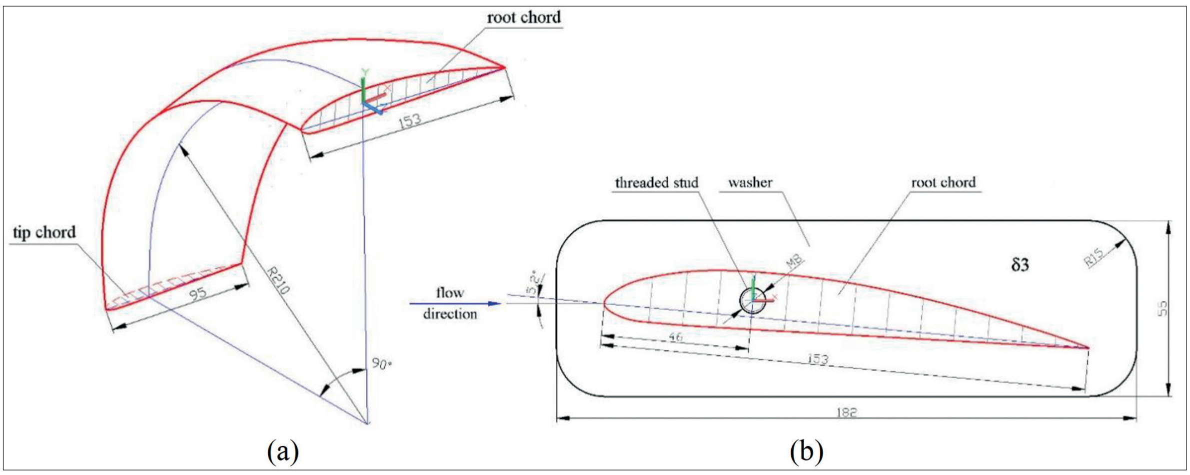

Fig. 8. Sketches showing (a) the mock-up of the arched wing and (b) the mounting scheme

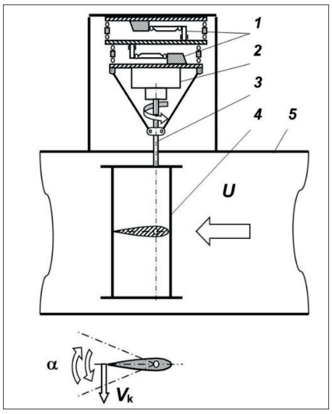

Fig. 9. Diagram showing the experimental setup and its arrangement in the working section of the hydrodynamic tube

The wing (4) was attached within the working section (5) of the hydrodynamic tunnel to the two-component strain gauge dynamometer (1). The wing's rotation about the transverse axis Z (3) was achieved using an electromechanical actuator (2).

In oscillatory mode, the electromechanical mechanism moved the wing in such a way that its angle of rotation varied over time according to the harmonic law $\alpha\ (t) = \beta \sin \omega t$, where ω is the angular frequency of oscillation, and β is the amplitude of the angular oscillations. The wing oscillation frequency f could be adjusted within the range 0.2–2.0 Hz during the experiments.

The design of the tensile dynamometer suspension involved a sharply directed minimum stiffness in a mutually perpendicular direction, to ensure the almost complete absence of mutual influence between the X and Y components. The measurement error of hydrodynamic forces on this experimental setup did not exceed 3%, and the rotation angle error did not exceed ± 0.2°.

Calibration of the two-component strain gauge platform and the oscillating unit with rotation angle sensors was performed directly before testing, on a special calibration stand. Fig. 10 shows the assembled experimental setup on the calibration stand. During the experiments, the hydrodynamic forces acting on the wing mock-up (lift and drag forces) were measured in the velocity coordinate system. The flow velocity in the hydrodynamic facility was measured using a Pitot tube with a Motorola differential pressure sensor MPX5010 DP, with measurement accuracy 2.5% V_{FSS}.

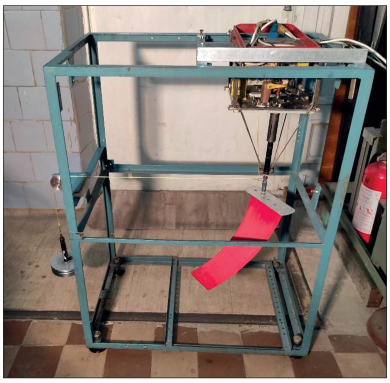

Fig. 10. Assembled experimental setup on the calibration stand

Registration of the hydrodynamic forces acting on the wing model, the angle of attack of the wing, and the flow velocity was carried out using a digital oscilloscope (ROHDE & SCHWARZ RTB 2004) with a data logging function connected to a computer.

The hydrodynamic force coefficients acting on the wing mock-up were determined as follows:

– Drag force coefficient

$$C_x = \frac{2 \cdot Rx}{\rho \cdot U^2 \cdot A_R}, \quad (11)$$

where:

Rx –registered drag force;
ρ – mass density of water;
U – velocity of the water flow in the hydrodynamic tunnel;
A_R – the projected wing planform area.

The lift force coefficient was obtained as

$$C_y = \frac{2 \cdot Py}{\rho \cdot U^2 \cdot A_R}, \quad (12)$$

where Py is the registered lift force.

The velocity of water flow in the hydrodynamic tube during the experiments was U = 1.55 m/s, which at a water temperature of t = 14.8°C corresponded to a Reynolds number of $Re = (U{\cdot}b_{mac}/\nu) = 1.65{\cdot}10^5$ (where ν = 1.162 m²/s is the kinematic viscosity of water), calculated based on the mean aerodynamic chord length.

As a result of this series of experiments, the dependencies of the hydrodynamic force coefficients on the wing's angle of rotation were constructed in graphical form. During the tests, the oscillation mechanism of the experimental setup was adjusted to provide a wing rotation angle in the range ±15°. The wing model was mounted on the rotation shaft so that the angle of attack in the flow ranged from +0.5° to +30.5° with respect to the wing chord line. Table 2 presents the results of the wing mock-up tests in the hydrodynamic tunnel. The Table also includes the value of the aerodynamic efficiency coefficient (lift-drag ratio) for the wing, $K = Cy/Cx$.

After detailed verification and calibration of the experimental setup, repeated tests were conducted on two geometrically similar wing models. Wing mock-up No. 1 had a rough surface, while No. 2 had a polished surface. The quality of polishing approximated a hydrodynamically smooth surface, where the average height of the surface roughness protrusions was less than the thickness of the viscous sublayer of the boundary layer. To achieve this surface quality, in accordance with the recommendations in [20], the surface of the model was polished with P360 emery paper.

Table 3 presents the test results for wing models No. 1 and No. 2 in the hydrodynamic tube. The Table also includes the aerodynamic efficiency (lift-drag ratio), defined as $K = Cy/Cx$.

The graphs also include vertical error bars representing 5% measurement uncertainty.

DISCUSSION

The test results for wing mock-up No. 1 in the hydrodynamic tunnel showed that for the angle of attack of up to 18°, flow without separation was established, and the lift coefficient was directly proportional to the angle of attack of the wing $Cy = f(\alpha)$.

Tab. 2. Test results for the wing model in the hydrodynamic facility

Initial data:		
Water temperature in the tunnel	°C	14.8
Kinematic viscosity coefficient of water	m^2/s	1.62E-06
Flow velocity	m/s	1.55
Mean aerodynamic chord of the wing	m	0.124
Wing planform area	m^2	0.0426
Reynolds number	–	$1.65 \cdot 10^5$

Angle of attack, deg	*Cy*	*Cx*	*K*
0.50	0.103	0.027	3.75
2.37	0.178	0.030	6.04
6.95	0.364	0.033	10.98
10.68	0.532	0.046	11.60
15.78	0.760	0.073	10.48
19.03	0.821	0.089	9.19
22.76	0.923	0.132	6.99
24.60	0.872	0.175	5.00
27.89	0.905	0.240	3.77
30.24	0.867	0.258	3.36

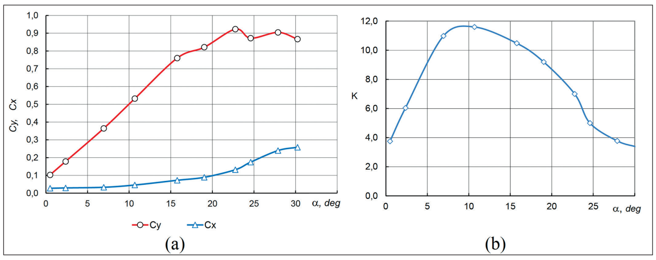

Fig. 11 shows the test results of the wing mock-up in the hydrodynamic tube in graphical form

The maximum lift coefficient reached values of 0.9.

The test results for wing mock-up No.2 in the hydrodynamic tunnel indicated that there was a linear relationship between the lift coefficient $Cy = f(\alpha)$ and the wing angle of attack, extending up to angles of attack of nearly 25°, with the maximum lift coefficient reaching a value of 1.0.

Tab. 3. Test results for wing models in the hydrodynamic facility

Initial data:			
Parameter	Units	Wing No. 1	Wing No. 2
Water temperature in the tunnel	°C	20.0	21.0
Kinematic viscosity coefficient of water	m^2/s	1.00E-06	0.986E-06
Flow velocity	m/s	1.51	1.47
Mean aerodynamic chord of the wing	m	0.124	0.124
Wing planform area	m^2	0.0426	0.0426
Reynolds number	–	$1.86 \cdot 10^5$	$1.85 \cdot 10^5$

	Wing No. 1			Wing No. 1		
Angle of attack, deg	*Cy*	*Cx*	*K*	*Cy*	*Cx*	*K*
0.50	0.101	0.033	3.061	0.090	0.032	2.80
1.44	0.146	0.033	4.431	0.135	0.032	4.21
2.38	0.172	0.033	5.224	0.163	0.032	5.08
3.31	0.212	0.033	6.430	0.196	0.032	6.13
5.19	0.271	0.038	7.132	0.256	0.032	7.99
7.53	0.373	0.045	8.226	0.357	0.038	9.51
10.34	0.468	0.056	8.295	0.459	0.050	9.24
15.50	0.639	0.084	7.565	0.630	0.074	8.48
18.31	0.743	0.103	7.224	0.745	0.095	7.86
21.12	0.824	0.122	6.756	0.837	0.114	7.31
23.47	0.874	0.136	6.404	0.906	0.134	6.76
25.34	0.900	0.173	5.201	0.964	0.151	6.39
27.22	0.808	0.198	4.081	1.011	0.183	5.52
28.62	0.810	0.234	3.464	1.008	0.230	4.38
29.56	0.827	0.307	2.692	0.962	0.242	3.98
30.50	0.749	0.340	2.202	0.967	0.264	3.66

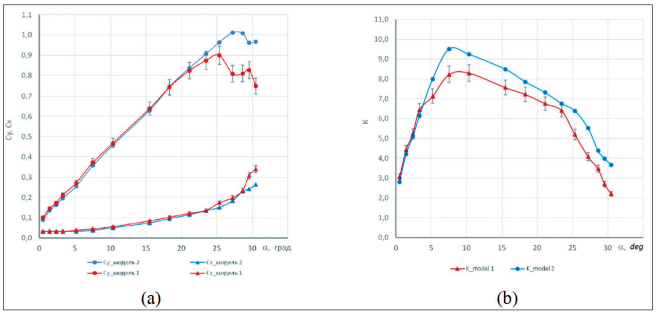

Fig. 12 presents combined graphs of the hydrodynamic characteristics of the wing models

CONCLUSION

The drag coefficient $Cy = f(\alpha)$ for wing mock-up No. 2 was somewhat lower, which resulted in a higher hydrodynamic efficiency $K = f(\alpha)$ for this model. The maximum hydrodynamic efficiency was achieved at angles of attack around 7°.

Torque issues in the design of towed underwater vehicles of this type are important, and a further study of motion stability will be a separate subject for future research.

REFERENCES

1. Blintsov OV, Sirivchuk AS. Kontseptsiia robotyzovanoho monitorynhu pidvodnoho seredovyshcha na osnovi zastosuvannia pryviaznykh pidvodnykh aparativ // East European Journal of Advanced Technologies – Kharkiv. №6/3(72), 2014. – C. 16-21.
2. Sun Q, Xu S, Sun T, Lu F, Dong P, Chang J. Design and experiment of a long range autonomous underwater vehicle for ocean acoustic data observation. Polish Maritime Research 2025, Vol. 32, no. 1, pp. 67-70. https://doi.org/10.2478/pomr-2025-0006
3. Zhao Q, Yang T, Tang G, Yang Y, Luan Y, Wang G, Wan T, Xu M, Li S, Xie G. Hierarchical model for an AUV swarm with a leader. Polish Maritime Research 2025, Vol. 32, no. 1, pp. 71-80. https://doi.org/10.2478/pomr-2025-0007

4. Blintsov VS, Nadtochyi AV. Humanitarne rozminuvannia milkovodnykh akvatorii: tekhnolohii ta robototekhnichne zabezpechennia. /"Shipbuilding and maritime infrastructure", 2024. Release №1(18). – C. 4-10. DOI https://doi.org/10.15589/smi2024.1(18).01

5. Blintsov V, Maidaniuk P, Sirivchuk A. Improvement of technical supply of projects of robotized monitoring of underwater conditions in shallow water areas. EUREKA: Physics and Engineering 2019, no. 3, pp. 41-49. DOI: 10.21303 / 2461-4262.2019.00893

6. Chen G, Chen W, Wang Z, Guo T, Xia X, Xu L. Design and Dynamic Performance Research of Underwater Inspection Robots. Wireless Communications and Mobile Computing. Volume 2022, Article ID 3715514, 13 pages. https://doi.org/10.1155/2022/3715514

7. Nishida Y, Kojima J, Ito Y, Tamura K, Sugimatsu H, Kim K. Development of an autonomous buoy system for AUV. In OCEANS 2015, Genova, Italy : IEEE. – 18-21 May 2015, Electronic ISBN:978-1-4799-8736-8. DOI: 10.1109/OCEANS-Genova.2015.7271614

8. Underwater Communication. https://waterlinked.com/applications/underwater-communication

9. Talebi M, Mahmud S, Khalifa A, Jahidul Islam M. BlueME: Robust underwater robot-to-robot communication using compact magnetoelectric antennas. Department of ECE, University of Florida, USA. https://www.researchgate.net/publication/385823509_BlueME_Robust_Underwater_Robot-to-Robot_Communication_Using_Compact_Magnetoelectric_Antennas

10. Radio Buoy. Gaymarine Electronic Products. https://www.gaymarine.it/en/accessories/radiobuoy

11. Pranddtl L. Gidroaeromekhanika. – Izhevsk : Research Center "Regular and Chaotic Dynamics". 2000.

12. Kitaev N. Samoleti s arochnim krilom. URL: http://savenergy.info/page/arched-wing-aircraft/

13. Slizhevskii NB, Korol YuM, Sokolik MG. Gidrodinamicheskii raschet samokhodnikh podvodnikh apparatov: Uchebnoe posobie. – Nikolaev : USMTU. 2000.

14. Kashafutdinov ST, Lushin VN. Atlas aerodinamicheskikh kharakteristik krilovikh profilei. –Siberian Scientific Research Institute of Aviation named after S.A. Chaplygin. 1994.

15. Kumar K, Zindani D, Roy AK. Working with ANSYS: A tutorial approach. IK International; 2017.

16. Madenci E, Guven I. Finite element method and applications in engineering using ANSYS. Springer London; 2015.

17. Kayan VP, Pyatetskii VE. Biogidrodinamicheskaya ustanovka zamknutogo tipa dlya issledovaniya gidromekhaniki plavaniya morskikh zhivotnikh. // Bionics , Kyiv, rel. 5. 1971.

18. Yegorov VI. Podvodnie buksiruemie sistemi. - Leningrad: Shipbuilding . 1981.

19. Korobov VI. Hydrodynamics of oscillating wing on the pitch angle. Proceedings of the National Aviation University, N2(71), 2017, pp. 70-75. DOI: 10.18372/2306-1472.71.11749

20. Ship Models. ITTC Recommended Procedures and Guidelines No. 7.5-01-01-01, 26th ITTC 2011. https://ittc.info/media/1201/75-01-01-01.pdf